Pseudoscalar and vector meson form factors from lattice QCD

J. N. Hedditch,[1] W. Kamleh,[1] B. G. Lasscock,[1] D. B. Leinweber,[1] A. G. Williams,[1] and J. M. Zanotti[2]

[1]*Department of Physics and Mathematical Physics and Special Research Centre for the Subatomic Structure of Matter, University of Adelaide, 5005, Australia*

[2]*School of Physics, University of Edinburgh, Edinburgh EH9 3JZ, United Kingdom*

(Received 14 March 2007; published 31 May 2007)

We present a study of the pseudoscalar and vector meson form factors, calculated using the fat-link irrelevant clover (FLIC) action in the framework of quenched lattice QCD. Of particular interest is the determination of a negative quadrupole moment, indicating that the ρ meson is not spherically symmetric.

DOI: 10.1103/PhysRevD.75.094504 PACS numbers: 12.38.Gc, 14.40.Aq

I. INTRODUCTION

The important role that electromagnetic form factors play in our understanding of hadronic structure has been well documented for more than 50 years. The reason for their popularity is that they encode information about the shape of hadrons, and provide valuable insights into their internal structure in terms of quark and gluon degrees of freedom.

Most of the attention, both experimentally and theoretically, has focused on the electromagnetic form factors of the nucleon (see Refs. [1–5] for recent reviews). The electromagnetic form factors of pseudoscalar mesons, especially the pion, being the lightest QCD bound state, have also been studied extensively [6–11] in lattice QCD. More recently, there is a renewed interest in calculating the pion form factor on the lattice [12–18]. This is especially timely considering the new [19] and reanalysis of old [20] experimental data from JLab.

The vector meson form factors, on the other hand, have received less attention (see Refs. [21–25] for recent work). Of particular interest is the quadrupole moment of the ρ meson, where theoretical determinations can disagree by as much as a factor of 2 [25]. We aim to resolve this issue by performing the first direct lattice calculation of the ρ-meson quadrupole form factor. Charge and magnetic form factors are also calculated and from these we extract the relevant static quantities, namely, the mean square charge-radius and magnetic moment. We also analyze the dependence of light-quark contributions to these form factors on their environment and contrast these with a new calculation of the corresponding pseudoscalar-sector result.

Our aim is to reveal the electromagnetic structure of vector mesons and to study to what extent the qualitative quark model picture is consistent with quenched lattice QCD. Interestingly, it has been shown in a lattice calculation by Alexandrou *et al.* [26] that the distribution of charge in the vector meson is oblate, and therefore not consistent with the picture of a quark antiquark in relative S-wave. By calculating the vector meson quadrupole form factor we make a direct comparison with the findings of Ref. [26].

For each observable we calculate the quark sector contributions separately. Using this additional information we examine the environmental sensitivity of the light-quark contributions to the pseudoscalar and vector meson charge radii. We also evaluate the dominance of the light quark contributions to the K and K^*.

This paper builds on the preliminary work presented in Ref. [27]. In Sec. II A we introduce the theoretical formalism of meson form factors, including the techniques required to extract them from a lattice calculation. Section III contains details of our lattice simulation, while in Sec. IV we present and discuss our results for both pseudoscalar and vector mesons. Finally, in Sec. V we summarize our findings and discuss future work.

II. THEORETICAL FORMALISM

A. Meson form factors

Meson form factors are extracted from matrix elements involving the vector (electromagnetic) current

$$\langle M(\vec{p}')|J^{\alpha}|M(\vec{p})\rangle, \tag{1}$$

where $M(\vec{p})$ ($M(\vec{p}')$) denotes a meson state with initial (final) momentum $\vec{p}$ ($\vec{p}'$). The momentum transfer is $q_\mu = (p'_\mu - p_\mu)$.

For a pion, the matrix element in Eq. (1) is described by a single form factor

$$\langle \pi(\vec{p}')|J^{\alpha}|\pi(\vec{p})\rangle = \frac{1}{2\sqrt{E_\pi(\vec{p})E_\pi(\vec{p}')}}[p^{\alpha} + p^{\alpha\prime}]F_\pi(Q^2), \tag{2}$$

where $Q^2 = -q^2$ is the invariant momentum transfer, and the energy of the pion with momentum $\vec{p}$ is $E_\pi(\vec{p}) = \sqrt{m_\pi^2 + \vec{p}^2}$. Here we adopt the notation of Bjorken and Drell [28] utilizing the Dirac representation for gamma matrices, a Minkowski-style metric, and $q^2 = (q^0)^2 - (\vec{q})^2$. The formula for the kaons are exactly analogous. The ρ-meson, on the other hand, is spin-1 and is described by three form factors [29],

$$\langle \rho(\vec{p}', s')|J^{\alpha}|\rho(\vec{p}, s)\rangle = \frac{1}{2\sqrt{E_\rho(\vec{p})E_\rho(\vec{p}')}} \times \epsilon'^{\star}_{\tau}(p', s')J^{\tau\alpha\sigma}(p', p)\epsilon_{\sigma}(p, s) \tag{3}$$

where ϵ and ϵ' are the initial and final polarization vectors, respectively, and

$$J^{\tau\alpha\sigma}(p', p) = -\Big\{G_1(Q^2)g^{\tau\sigma}[p^{\alpha} + p^{\alpha\prime}] + G_2(Q^2)[g^{\alpha\sigma}q^{\tau} - g^{\alpha\tau}q^{\sigma}] - G_3(Q^2)q^{\sigma}q^{\tau}\frac{p^{\alpha} + p^{\alpha\prime}}{2m_\rho^2}\Big\}. \tag{4}$$

The covariant vertex functions $G_{1,2,3}$ can be rewritten in terms of the Sachs charge, magnetic and quadrupole form factors [29,30],

$$G_Q(Q^2) = G_1(Q^2) - G_2(Q^2) + (1 + \eta)G_3(Q^2) \tag{5}$$

$$G_M(Q^2) = G_2(Q^2) \tag{6}$$

$$G_C(Q^2) = G_1(Q^2) + \tfrac{2}{3}\eta G_Q(Q^2), \tag{7}$$

where m_ρ is the mass of the vector meson system calculated on the lattice and $\eta = Q^2/4m_\rho^2$.

The charge q_ρ, magnetic moment μ_ρ, and quadrupole moment Q_ρ are then extracted from G_C, G_M, and G_Q, respectively, at zero momentum transfer

$$eG_C(0) = q_\rho \tag{8}$$

$$eG_M(0) = 2m_\rho\mu_\rho \tag{9}$$

$$eG_Q(0) = m_\rho^2 Q_\rho. \tag{10}$$

The formulas for the K^* are exactly analogous.

B. Meson form factors on the lattice

In practice, we work with a Hermitian gamma-matrix representation in our lattice simulations and select the Pauli representation of Sakurai [31] for our correlation function construction. This representation utilizes a Euclidean-style metric, $\delta_{\mu\nu}$.

Since the Dirac and Pauli representations of the gamma matrices differ by factors of i in the spatial components, it is a simple matter to transform our Euclidean-time lattice correlation functions from the Pauli representation to the Dirac representation which incorporates a Minkowski-style metric. In this way we may connect the Euclidean-time correlation functions to the results of Sec. II A.

Thus, the matrix elements in Eqs. (2) and (3) are obtained from ratios of three-point and two-point correlation functions

$$R^{\alpha}(p', p) = \sqrt{\frac{\langle G^{\alpha}(\vec{p}', \vec{p}, t_2, t_1)\rangle\langle G^{\alpha}(\vec{p}, \vec{p}', t_2, t_1)\rangle}{\langle G(\vec{p}', t_2)\rangle\langle G(\vec{p}, t_2)\rangle}} \tag{11}$$

for pseudoscalar mesons, and

$$R^{\alpha}_{\mu\nu}(p', p) = \sqrt{\frac{\langle G^{\alpha}_{\mu\nu}(\vec{p}', \vec{p}, t_2, t_1)\rangle\langle G^{\alpha}_{\nu\mu}(\vec{p}, \vec{p}', t_2, t_1)\rangle}{\langle G_{\mu\mu}(t_2, \vec{p}')\rangle\langle G_{\nu\nu}(t_2, \vec{p})\rangle}} \tag{12}$$

for vector mesons. Note repeated indices are not summed over. The square root in Eqs. (11) and (12) spoils the covariant/contravariant nature of $R^{\alpha}_{\mu\nu}$ and no meaning should be attached to the location of these indices. However, we prefer to use this notation due to the close connection with $G^{\alpha}_{\mu\nu}$.

The two-point correlation function for the pseudoscalar mesons is

$$G(t_2, \vec{p}) = \sum_{\vec{x}_2} e^{-i\vec{p}\cdot\vec{x}_2}\langle\Omega|\chi(x_2)\chi^{\dagger}(0)|\Omega\rangle. \tag{13}$$

Similarly for the vector mesons,

$$G_{\mu\nu}(t_2, \vec{p}) = \sum_{\vec{x}_2} e^{-i\vec{p}\cdot\vec{x}_2}\langle\Omega|\chi_\mu(x_2)\chi^{\dagger}_\nu(0)|\Omega\rangle. \tag{14}$$

The three-point correlation function for the pseudoscalar meson is

$$G^{\alpha}(t_2, t_1, \vec{p}', \vec{p}) = \sum_{\vec{x}_1,\vec{x}_2} e^{-i\vec{p}'\cdot(\vec{x}_2-\vec{x}_1)} \times e^{-i\vec{p}\cdot\vec{x}_1}\langle\Omega|\chi(x_2)J^{\alpha}(x_1)\chi^{\dagger}(0)|\Omega\rangle. \tag{15}$$

Similarly the three-point function for the vector meson is

$$G^{\alpha}_{\mu\nu}(t_2, t_1, \vec{p}', \vec{p}) = \sum_{\vec{x}_1,\vec{x}_2} e^{-i\vec{p}'\cdot(\vec{x}_2-\vec{x}_1)} \times e^{-i\vec{p}\cdot\vec{x}_1}\langle\Omega|\chi_\mu(x_2)J^{\alpha}(x_1)\chi^{\dagger}_\nu(0)|\Omega\rangle. \tag{16}$$

The Lorentz indices μ and ν are only present for the vector mesons, while α is the index of the electromagnetic current.

The ratios in Eqs. (11) and (12) are constructed in such a way as to remove the time-dependence and constants of normalization from the correlation functions at large time separations, t_1 and $t_2 - t_1$.

These ratios differ subtly from previous work [32], in that we are explicitly enforcing the parity of the terms through the choice of momenta (p', p) and (p, p') vs (p', p) and $(-p, -p')$. This requires two three-point propagators (with momentum-transfer q and $-q$) for each configuration. However with the well established technique of averaging over U and U^* configurations [32,33], there is no additional cost.

1. π-meson case

Since the pion has zero spin, the vertex is extraordinarily simple and takes the form given in Eq. (2). Here we show how this function is extracted from the ratio Eq. (11) by evaluating the correlation functions at large Euclidean times.

First we define the matrix elements as,

$$\begin{aligned}\langle\Omega|\chi_\mu(0)|\pi(\vec{p})\rangle &= \frac{1}{\sqrt{2E_\pi(\vec{p})}}\lambda_\pi(\vec{p}),\\ \langle\pi(\vec{p})|\chi^\dagger_\mu(0)|\Omega\rangle &= \frac{1}{\sqrt{2E_\pi(\vec{p})}}\bar{\lambda}_\pi(\vec{p}).\end{aligned} \tag{17}$$

Here $\lambda_\pi(\vec{p})$ and $\bar{\lambda}_\pi(\vec{p})$ are the couplings of the interpolator to the pion with momentum $\vec{p}$ at the sink and source, respectively. The momentum dependence allows for the use of smeared fermion sources and sinks. The bar allows for different amounts of smearing at the source and sink.

By inserting a complete set of energy and momentum states into Eq. (13), we can show that at large Euclidean time,

$$\lim_{t_2\to\infty} G(t_2,\vec{p}) = \frac{e^{-E_\pi(\vec{p})t_2}}{2E_\pi(\vec{p})}\lambda_\pi(\vec{p})\bar{\lambda}_\pi(\vec{p}). \tag{18}$$

Following the same treatment, one can show that the three-point function Eq. (15) at large Euclidean time is

$$\begin{aligned}\lim_{t_1,t_2-t_1\to\infty} G^\alpha(t_2,t_1,\vec{p}',\vec{p}) = &\frac{e^{-E_\pi(\vec{p}')(t_2-t_1)}e^{-E_\pi(\vec{p})t_1}}{2\sqrt{E_\pi(\vec{p})E_\pi(\vec{p}')}}\lambda_\pi(\vec{p}')\\ &\times\langle\pi(\vec{p}')|J^\alpha(0)|\pi(\vec{p})\rangle\bar{\lambda}_\pi(\vec{p}).\end{aligned} \tag{19}$$

Substituting these expressions into Eq. (11) and using Eq. (2), the ratio $R^\alpha(p',p)$ simply reduces to

$$R^\alpha(p',p) = \frac{1}{2\sqrt{E_\pi(\vec{p})E_\pi(\vec{p}')}}[p^\alpha + p^{\alpha\prime}]F_\pi(Q^2), \tag{20}$$

such that the large Euclidean time limits of the ratio R^α is a direct measure of $F_\pi(Q^2)$ up to kinematical factors.

2. ρ-meson case

Following [29], we define the matrix element of the electromagnetic current for ρ-meson in terms of the covariant vertex functions $G_{1,2,3}$ as in Eqs. (3) and (4).

The analogues of the matrix elements in Eq. (17) are

$$\begin{aligned}\langle\Omega|\chi_\mu(0)|\rho(\vec{p},s)\rangle &= \frac{1}{\sqrt{2E_\rho(\vec{p})}}\lambda_\rho(\vec{p})\epsilon_\mu(p,s)\\ \langle\rho(\vec{p},s)|\chi^\dagger_\nu(0)|\Omega\rangle &= \frac{1}{\sqrt{2E_\rho(\vec{p})}}\bar{\lambda}_\rho(\vec{p})\epsilon^\star_\nu(p,s).\end{aligned} \tag{21}$$

The polarization vectors obey the transversality condition

$$\sum_s \epsilon_\mu(p,s)\epsilon^\star_\nu(p,s) = -\left(g_{\mu\nu} - \frac{p_\mu p_\nu}{m_\rho^2}\right), \tag{22}$$

because the vector meson current is a conserved current.

The evaluation of the two- and three-point functions proceeds as for our discussion of the pion. However the completeness relation includes a sum over spin-states. Using the transversality condition Eq. (22) the analogue of Eq. (18) becomes

$$\begin{aligned}\lim_{t_2\to\infty} G(t_2,\vec{p}) &= \sum_s \frac{e^{-E_\rho(\vec{p})t_2}}{2E_\rho(\vec{p})}\lambda_\rho(\vec{p})\bar{\lambda}_\rho(\vec{p})\epsilon_\mu(p,s)\epsilon^\star_\nu(p,s)\\ &= -\frac{e^{-E_\rho(\vec{p})t_2}}{2E_\rho(\vec{p})}\lambda_\rho(\vec{p})\bar{\lambda}_\rho(\vec{p})\left(g_{\mu\nu} - \frac{p_\mu p_\nu}{m_\rho^2}\right).\end{aligned} \tag{23}$$

Similarly, using Eq. (3) we can evaluate the Euclidean-time three-point function,

$$\begin{aligned}\lim_{t_1,t_2-t_1\to\infty} G^\alpha_{\mu\nu}(t_2,t_1,\vec{p}',\vec{p}) &= \sum_{s,s'}\frac{e^{-E_\rho(\vec{p}')(t_2-t_1)}e^{-E_\rho(\vec{p})t_1}}{4E_\rho(\vec{p})E_\rho(\vec{p}')}\lambda_\rho(\vec{p}')\epsilon_\mu(p',s')\epsilon'^\star_\tau(p',s')J^{\tau\alpha\sigma}(p',p)\epsilon_\sigma(p,s)\bar{\lambda}_\rho(\vec{p})\epsilon^\star_\nu(p,s)\\ &= \frac{e^{-E_\rho(\vec{p}')(t_2-t_1)}e^{-E_\rho(\vec{p})t_1}}{4E_\rho(\vec{p})E_\rho(\vec{p}')}\lambda_\rho(\vec{p}')\bar{\lambda}_\rho(\vec{p})\left(g_{\mu\tau} - \frac{p'_\mu p'_\tau}{m_\rho^2}\right)J^{\tau\alpha\sigma}\left(g_{\sigma\nu} - \frac{p_\sigma p_\nu}{m_\rho^2}\right).\end{aligned} \tag{24}$$

Inserting the above expressions into the ratio in Eq. (12), together with our choice of momentum used in the simulations, namely $p' = (E_\rho, p_x, 0, 0)$ $(E_\rho = \sqrt{m_\rho^2 + p_x^2})$ and $p = (m_\rho, 0, 0, 0)$, it is possible to express $R^\alpha_{\mu\nu}$ in terms of the Sachs form factors,

$$R^0_{11} = \frac{p_x^2}{3m_\rho\sqrt{E_\rho m_\rho}}G_Q(Q^2) + \frac{E_\rho + m_\rho}{2\sqrt{E_\rho m_\rho}}G_C(Q^2), \qquad R^0_{22} = R^0_{33} = -\frac{p_x^2}{6m_\rho\sqrt{E_\rho m_\rho}}G_Q(Q^2) + \frac{E_\rho + m_\rho}{2\sqrt{E_\rho m_\rho}}G_C(Q^2),$$
$$R^3_{13} = R^3_{31} = \frac{p_x}{2\sqrt{E_\rho m_\rho}}G_M(Q^2).$$

We remind the reader that the square root in Eqs. (11) and (12) spoils the covariant/contravariant nature of $R^{\alpha}_{\mu\nu}$ and no meaning can attached to the location of these indices. The notation is simply a reflection of the close connection to $G^{\alpha}_{\mu\nu}$, where the index position is significant due to our use of the common Bjorken and Drell notation to express the phenomenology of vector meson form factors.

The individual form factors are isolated as follows:

$$G_C(Q^2) = \frac{2}{3}\frac{\sqrt{E_\rho m_\rho}}{E_\rho + m_\rho}(R^0_{11} + R^0_{22} + R^0_{33}), \tag{25}$$

$$G_M(Q^2) = \frac{\sqrt{E_\rho m_\rho}}{p_x}(R^3_{13} + R^3_{31}), \tag{26}$$

$$G_Q(Q^2) = \frac{m_\rho\sqrt{E_\rho m_\rho}}{p_x^2}(2R^0_{11} - R^0_{22} - R^0_{33}). \tag{27}$$

While we have used the subscript ρ to denote a vector meson, the results are applicable to vector mesons in general, including the K^* for example.

C. Extracting static quantities

The mean squared charge radius $\langle r^2\rangle$ is obtained from the charge form factor through the following relation,

$$\langle r^2\rangle = -6\frac{\partial}{\partial Q^2}G(Q^2)|_{Q^2=0}. \tag{28}$$

To calculate the derivative the monopole form is used,

$$G_C(Q^2) = \left(\frac{1}{\frac{Q^2}{\Lambda^2}+1}\right). \tag{29}$$

Λ is referred to as the monopole mass. Inserting this form into Eq. (28) and rearranging provides

$$\langle r^2\rangle = \frac{6}{Q^2}\left(\frac{1}{G_C(Q^2)} - 1\right), \tag{30}$$

valid for quantities with $G_C(Q^2 = 0) = 1$.

As mentioned in Sec. II A, the charge [Eq. (8)], magnetic moment ([Eq. (9)], and quadrupole moment [Eq. (10)] can be extracted from the Sachs form factors at zero momentum transfer. Since we perform our calculations at a single, finite value of Q^2, we will need to adjust our results to zero momentum transfer.

From studies of nucleon properties, it is observed that G_M and G_C have similar Q^2-scaling at small Q^2 [34]. In the following, we shall assume that this scaling also holds for quark contributions to mesons. If $G_C(0) = 1$, we have

$$G_M(0) \simeq \frac{G_M(Q^2)}{G_C(Q^2)}. \tag{31}$$

Whilst a similar scaling could be used to relate our quadrupole form factor to the quadrupole moment, we believe that the form factor at our small finite Q^2 ($\simeq 0.22$ GeV) will be of greater phenomenological interest. We note that for a positively charged meson a negative value of G_Q corresponds to an oblate deformation.

III. METHOD

The electromagnetic form factors are obtained using the three-point function techniques established by Leinweber, *et al.* in Refs. [32,35,36] and updated for smeared sources in Ref. [33]. Our quenched gauge fields are generated with the $\mathcal{O}(a^2)$ mean-field improved Luscher-Weisz plaquette plus rectangle gauge action [37] using the plaquette measure for the mean link. We use an ensemble of 379 quenched gauge field configurations on $20^3 \times 40$ lattices with lattice spacing $a = 0.128$ fm. The gauge field configurations are generated via the Cabibbo-Marinari pseudo-heat-bath algorithm [38] using a parallel algorithm with appropriate link partitioning [39].

We use the fat-link irrelevant clover (FLIC) Dirac operator [40] which provides a new form of nonperturbative $\mathcal{O}(a)$ improvement [41]. The improved chiral properties of FLIC fermions allow efficient access to the light quark-mass regime [42], making them ideal for dynamical fermion simulations now underway [43]. For the vector current, we an $\mathcal{O}(a)$-improved FLIC conserved vector current [33]. We use a smeared source at $t_2 = 8$. Complete simulation details are described in Ref. [33].

Table I provides the κ-values used in our simulations, together with the calculated pseudoscalar and vector meson masses. While we refer to m_π^2 in our figures and tables to infer the quark masses, we note that the critical value where the pion mass vanishes is $\kappa_{\rm cr} = 0.131\,35$. Importantly the vector mesons remain bound at all quark masses considered in this calculation due to finite volume effects. That is, the mass of the vector mesons is less than the energy of the lowest lying multihadron state with the appropriate quantum numbers.

The strange quark mass is chosen to be the third heaviest quark mass. This provides a pseudoscalar mass of 697 MeV which compares well with the experimental value of $(2M_K^2 - M_\pi^2)^{1/2} = 693$ MeV motivated by chiral perturbation theory. Two vector meson interpolating fields

TABLE I. Meson masses for the respective values of the hopping parameter κ.

κ	am_π	am_K	am_ρ	am_{K^*}
0.12780	0.5411(10)	0.4993(11)	0.7312(30)	0.7057(27)
0.12830	0.5013(11)	0.4782(11)	0.7067(36)	0.6933(40)
0.12885	0.4539(11)	0.4539(11)	0.6797(46)	0.6796(46)
0.12940	0.4014(12)	0.4285(11)	0.6537(49)	0.6668(47)
0.12990	0.3471(15)	0.4044(12)	0.6309(56)	0.6556(50)
0.13205	0.3020(19)	0.3862(13)	0.6160(64)	0.6484(52)
0.13060	0.2412(42)	0.3671(19)	0.6039(71)	0.6423(54)
0.13080	0.1968(52)	0.3574(16)	0.5982(80)	0.6393(56)

are considered, namely $\bar{q}\gamma_i q$ and $\bar{q}\gamma_i\gamma_4 q$. Since results for the two interpolators agree, we simply present the results for the $\bar{q}\gamma_i q$ interpolator, which displays a significantly stronger signal.

The error analysis of the correlation function ratios is performed via a second-order, single-elimination jackknife, with the χ^2 per degree of freedom ($\chi^2_{\rm dof}$) obtained via covariance matrix fits. We perform a series of fits through the ratios after the current insertion at $t = 14$. By examining the $\chi^2_{\rm dof}$ we are able to establish a valid window through which we may fit in order to extract our observables. In all cases, we required a value of $\chi^2_{\rm dof}$ no larger than 1.5. The values of the static quantities quoted in this paper on a per quark-sector basis correspond to values for single quarks of unit charge.

IV. RESULTS

A. Charge radii

We begin the discussion of our results with the charge radii of the vector and pseudoscalar mesons. From the quark model we would expect a hyperfine interaction between the quark and antiquark of the form $\frac{\vec{\sigma}_q\cdot\vec{\sigma}_{\bar{q}}}{m_q m_{\bar{q}}}$. The interaction is repulsive where the spins are aligned, as in the vector mesons, and attractive where the spins are anti-aligned, as in the pseudoscalar mesons. In Fig. 1 we show the charge radii of the vector and pseudoscalar mesons. For comparison the charge radius of the proton is also shown. Indeed we find that the charge radii of the vector mesons are consistently larger than the pseudoscalar mesons, and in fact similar to the charge radii of the proton, even at heavier quark masses. This is contrary to earlier lattice simulations with relatively small spatial extent [44], that have suggested that the π^+, ρ^+ and proton should have a very similar RMS charge radius at larger quark masses. It is possible that the agreement obtained in the previous study reflects finite-volume effects attendant with the use of a small spatial volume.

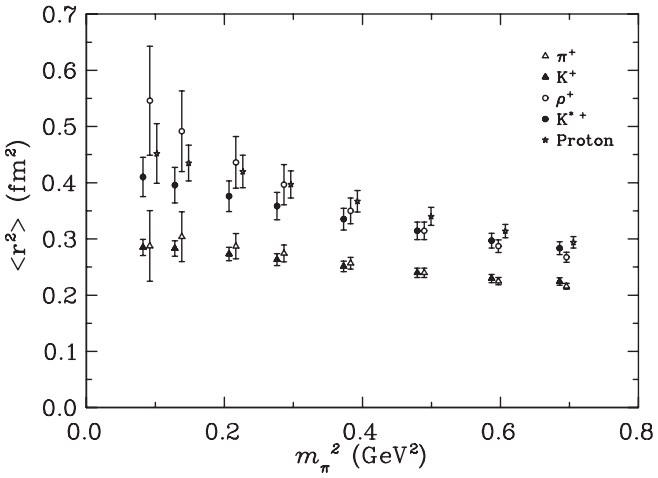

FIG. 1. Strange and nonstrange meson mean squared charge radii for charged pseudoscalar and vector mesons. We also include for comparison results for the proton taken from Ref. [33]. The π and ρ-meson results are centered on the relevant value of m_π^2, other symbols are offset horizontally for clarity.

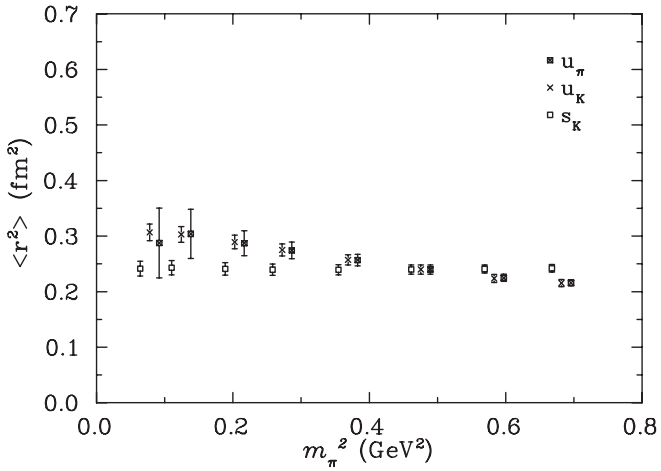

FIG. 2. The quark sector contributions to the mean squared charge radius of the pseudoscalar mesons. The symbols are offset horizontally for clarity.

By comparing the results for the up-quark contributions to the π and K (ρ and K^*) charge radii, it is possible to gain insights into the effect that the presence of a heavier strange-quark has on the lighter up-quark in pseudoscalar (vector) mesons. Figs. 2 and 3 show the quark sector contributions to the charge radii ($\langle r^2\rangle$) of the pseudoscalar and vector mesons, respectively. The quark sector contributions to the charge radii for the pseudoscalar and vector meson are recorded in Tables II and III. From Fig. 2, we find no evidence of environmental sensitivity in the light-quark contribution the pseudoscalar mesons. However in the vector sector, Fig. 3, we find a consistently broader

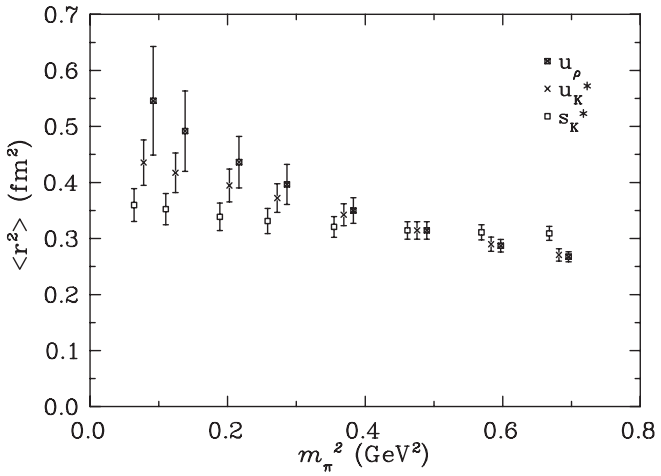

FIG. 3. As for Fig. 2 but for vector mesons.

TABLE II. Mean-square charge radius ($\langle r^2 \rangle$) for quarks of unit charge in units of fm^2. m_π^2 is given as a measure of the input quark mass.

m_π^2 (GeV^2)	u_π	u_K	s_K
0.6956(26)	0.216(5)	0.215(7)	0.242(7)
0.5970(26)	0.225(6)	0.224(7)	0.241(7)
0.4895(24)	0.240(8)	0.240(8)	0.240(8)
0.3828(23)	0.256(10)	0.257(9)	0.239(9)
0.2862(25)	0.274(14)	0.275(11)	0.239(10)
0.2166(27)	0.287(22)	0.289(12)	0.241(11)
0.1382(48)	0.304(44)	0.303(14)	0.243(13)
0.0920(49)	0.287(63)	0.306(15)	0.241(13)

TABLE III. Mean-square charge radius ($\langle r^2 \rangle$) for quarks of unit charge in units of fm^2.

m_π^2 (GeV^2)	u_ρ	u_{K^*}	s_{K^*}
0.6956(26)	0.268(9)	0.271(11)	0.309(12)
0.5970(26)	0.287(11)	0.290(13)	0.311(14)
0.4895(24)	0.315(16)	0.315(16)	0.315(16)
0.3828(23)	0.350(23)	0.342(20)	0.321(19)
0.2862(25)	0.397(36)	0.372(26)	0.331(23)
0.2166(27)	0.436(46)	0.395(30)	0.339(25)
0.1382(48)	0.492(72)	0.417(35)	0.353(28)
0.0920(49)	0.546(97)	0.436(41)	0.360(29)

distribution of up-quark charge in the ρ compared to the up-quark in the K^* at the smaller quark masses. The broadening of the charge distribution in the ρ is consistent with the hyperfine repulsion discussed above. The strange quark in the K^* shows a particularly interesting environment sensitivity. While the strange quark mass is held fixed, the distribution broadens as the light-quark regime is approached. This is consistent with the prediction of enhanced hyperfine repulsion as one of the quarks becomes light.

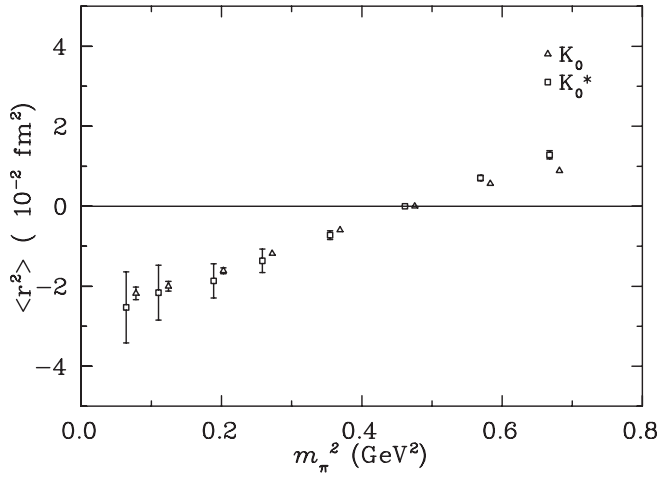

FIG. 4. The mean squared charge radii for the neutral K^0 and K^{0*}.

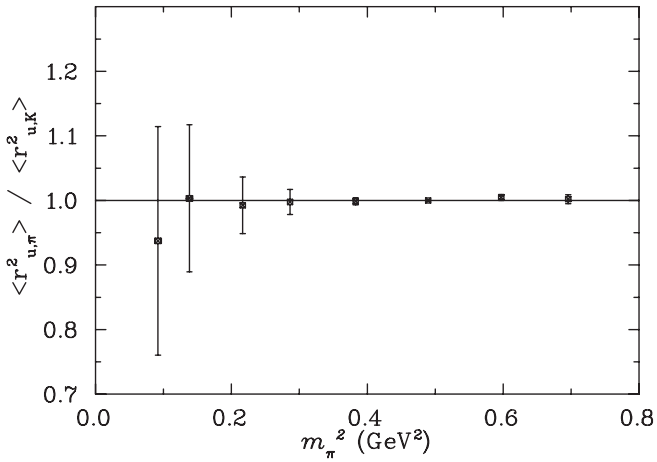

FIG. 5. The ratio of the light quark contributions to the π and K mean squared charge radius.

The strange neutral pseudoscalar and vector meson mean squared charge radii obtained from the weighted sum of the quark sector radii are displayed in Fig. 4. For the neutral strange mesons, we see a negative value for $\langle r^2 \rangle$, indicating that the negatively charged d-quark is lying further from the center of mass on average than the $\bar{s}$. We should expect just such a behavior for two reasons, both stemming from the fact that the $\bar{s}$ quark is considerably heavier than the d: the center of mass must lie closer to the $\bar{s}$, and the d-quark will also have a larger Compton wavelength. Of course with exact isospin symmetry in our simulations, the nonstrange charge neutral mesons have a zero electric charge radius.

To measure the environmental sensitivity of the light-quark sector more precisely, in Figs. 5 and 6 we show a fit to the ratio of the light-quark contributions to the pseudoscalar and vector mesons charge radii, respectively. The difference is striking: for the pseudoscalar case we see no environment-dependence at all, whereas in the vector case

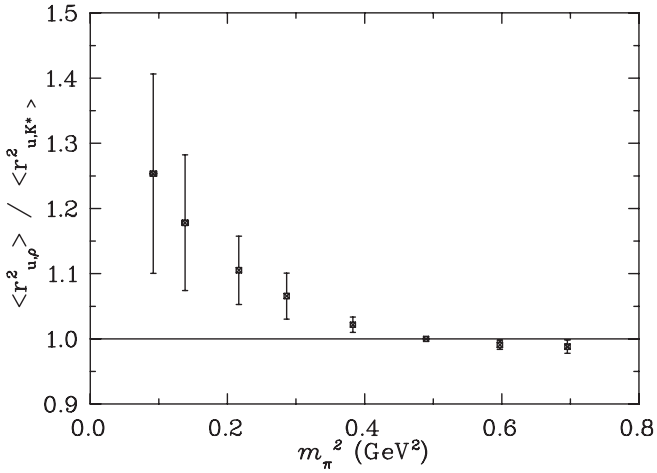

FIG. 6. As in Fig. 5 but for the vector mesons.

we see that the presence of a strange quark acts to heavily suppress the light charge distribution. This is the effect one predicts from a quark model, where the large mass of the s would act to suppress the hyperfine repulsion between the quark and antiquark. It is also qualitatively consistent with effective field theory where the couplings of the light mesons are suppressed by the presence of the strange quark.

B. Magnetic moments

In Fig. 7 we present our results for the magnetic moments of the vector mesons. At the $SU(3)_{\text{flavour}}$ limit, where we take the light quark flavours to have the same mass as the strange quark, quark model arguments suggest the magnetic moment for a ρ^+ should be -3 times the strange magnetic moment of the Λ (assuming no environmental dependence). According to the particle data group [45], the magnetic moment of the Λ is $-0.613\mu_N$. Therefore we would naively expect a value of $1.84\mu_N$ for the magnetic moment of the ρ^+, which is consistent with our findings.

In an earlier study, Anderson *et al.* [46] argued that the magnetic moment of the ρ-meson in natural magnetons (otherwise called the g-factor) should be approximately 2 at large quark masses. Converting our result to natural magnetons, we observe in Fig. 8 that our calculation of the ρ-meson g-factor (g_ρ) is fairly consistent with this. At light quark masses, however, we do see some evidence of chiral curvature, which would indicate that the linear chiral extrapolations of that paper should be considered with caution.

In Fig. 9 we present the quark sector contributions to the vector meson magnetic moments, the data is recorded in Table IV. Here we observe a similar scenario to that observed earlier in the charge radius discussion, namely, that the u-quark contribution to the K^* is consistently larger than the contribution from the heavier s-quark. We also find that the contribution of the u-quark to the magnetic moment of a vector meson is suppressed when it is an environment of a heavier s-quark compared to when it is in the presence of another light quark. This is further supported when we consider the ratio of the contributions of a u-quark to the magnetic moments of the ρ and K^* mesons,

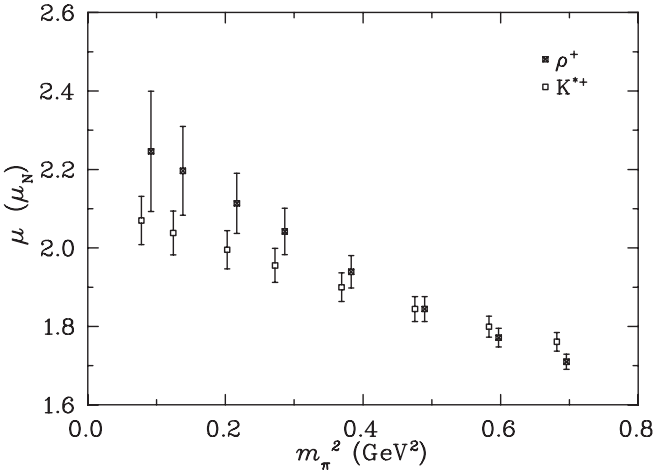

FIG. 7. Charged vector meson magnetic moments.

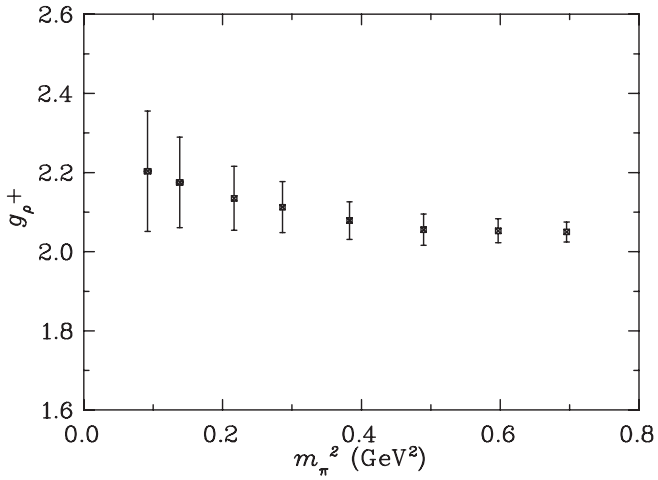

FIG. 8. The g-factor of the ρ meson.

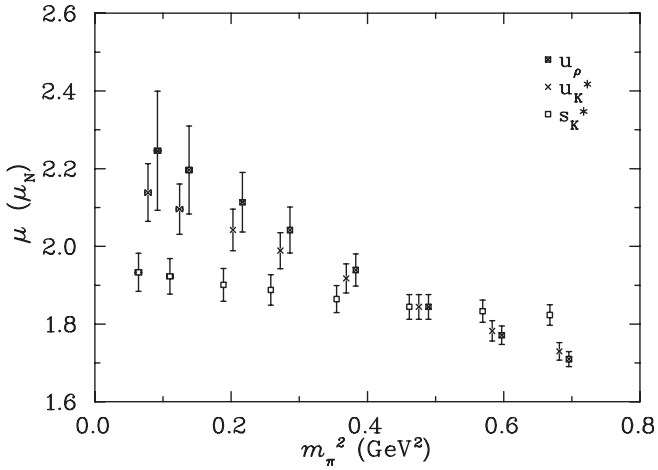

FIG. 9. Quark-sector contributions to the vector meson magnetic moments.

TABLE IV. Magnetic moment for quarks of unit charge inside a vector meson in units of nuclear magnetons μ_N.

m_π^2 (GeV^2)	u_ρ	u_{K^*}	s_{K^*}
0.6956(26)	1.71(2)	1.73(2)	1.82(3)
0.5970(26)	1.77(2)	1.78(3)	1.83(3)
0.4895(24)	1.84(3)	1.84(3)	1.84(3)
0.3828(23)	1.94(4)	1.92(4)	1.86(3)
0.2862(25)	2.04(6)	1.99(5)	1.88(4)
0.2166(27)	2.11(8)	2.04(5)	1.90(4)
0.1382(48)	2.20(11)	2.10(6)	1.92(5)
0.0920(49)	2.25(15)	2.14(7)	1.93(5)

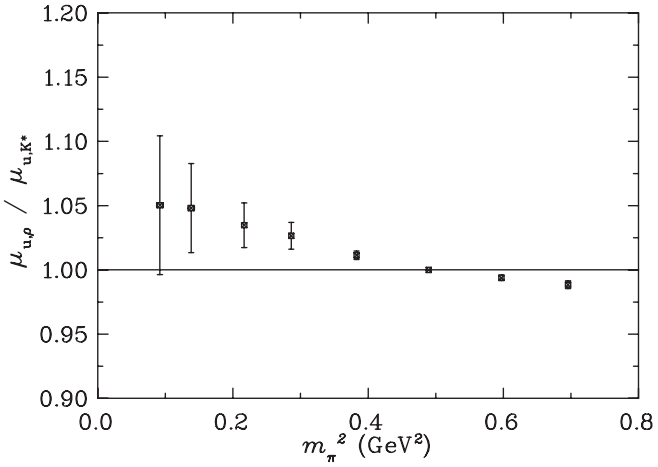

FIG. 10. The ratio of the light-quark contributions to the magnetic moment of the ρ and K^*.

displayed in Fig. 10. This ratio is clearly greater than 1 below the $SU(3)_{\text{flavour}}$ limit and is increasing for decreasing u-quark mass.

The magnetic moment of the vector meson, like the RMS charge radius, shows considerable environment dependence in the quark sector contributions. The larger contribution of a u-quark in a ρ relative to a K^* is consistent with what we have already observed with the RMS charge radius, as follows: since $\langle r^2 \rangle$ is larger for the u-quark in a ρ meson than for the u-quark in a K^*, the effective mass is reciprocally smaller for the u-quark in a ρ. This smaller effective mass gives rise in turn to a larger magnetic moment. Figure 10 shows this pattern. Figure 11 presents our results for the magnetic moment of the neutral K^{*0} meson. As the d-quark becomes lighter than the $\bar{s}$ we see the magnetic moment exhibiting a very linear negative slope. The magnitude of the magnetic moment is quite small, but clearly differentiable from zero everywhere except at the $SU(3)_{\text{flavour}}$ limit where symmetry forces it to be exactly zero.

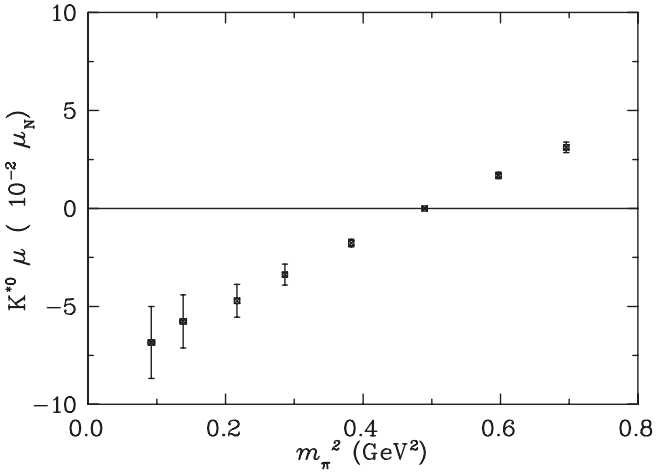

FIG. 11. Neutral K^*-meson magnetic moment.

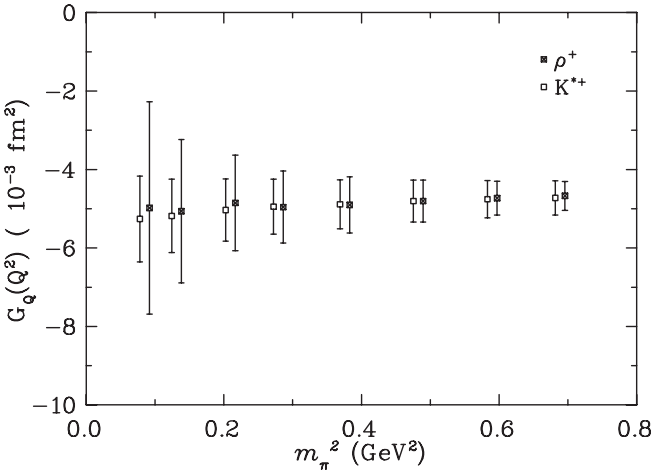

FIG. 12. Vector meson quadrupole form factors for ρ^+ and K^{*+}.

C. Quadrupole form factors

The quadrupole form factors of the ρ^+ and K^{*+} mesons are shown in Fig. 12. We find that the quadrupole form factor is less than zero, indicating that the spatial distribution of charge within the ρ and K^* mesons is oblate. This is in accord with the findings of Alexandrou *et al.* [26] who observed a negative quadrupole moment for spin ± 1 ρ-meson states in a density-density analysis. We note that in a simple quark model, a negative quadrupole form factor requires that the quarks possess an admixture of s- and d-wave functions.

The quark sector contributions to the quadrupole form factor are shown in Fig. 13. The corresponding data is contained in Table V. The flavour independence of the results is remarkable.

We also find that the ratio of the light-quark contributions to the quadrupole form factor, shown in Fig. 14, is consistent with one within our statistics. In Fig. 15, we

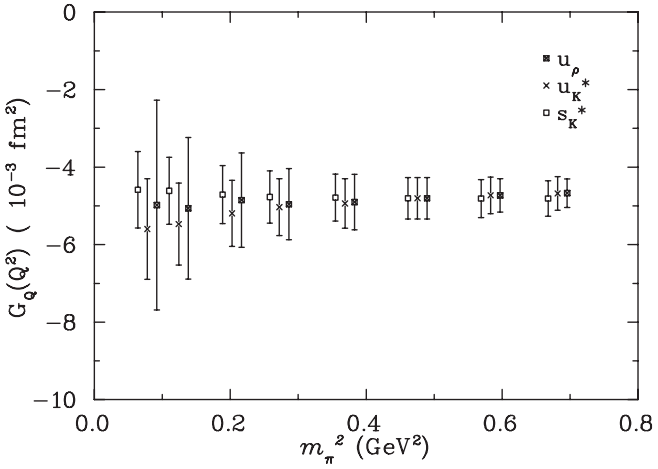

FIG. 13. Quark-sector contributions to the quadrupole form factors.

show the quadrupole form factor of the charge neutral K^{*0} meson. We find that the quadrupole moment of the K^{*0} is nontrivial but just outside the 1 standard deviation level. The chiral trend towards positive values reflecting the negative charge of the larger d-quark contributions.

TABLE V. The quadrupole form factor (in fm^2) for quarks of unit charge inside a vector meson.

m_π^2 (GeV)^2	u_ρ	u_{K^*}	s_{K^*}
0.6956(26)	−0.0047(4)	−0.0047(4)	−0.0048(5)
0.5970(26)	−0.0047(4)	−0.0047(5)	−0.0048(5)
0.4895(24)	−0.0048(5)	−0.0048(5)	−0.0048(5)
0.3828(23)	−0.0049(7)	−0.0049(6)	−0.0048(6)
0.2862(25)	−0.0050(9)	−0.0050(7)	−0.0048(7)
0.2166(27)	−0.0049(12)	−0.0052(9)	−0.0047(7)
0.1382(48)	−0.0051(19)	−0.0055(11)	−0.0046(9)
0.0920(49)	−0.0050(27)	−0.0056(13)	−0.0046(10)

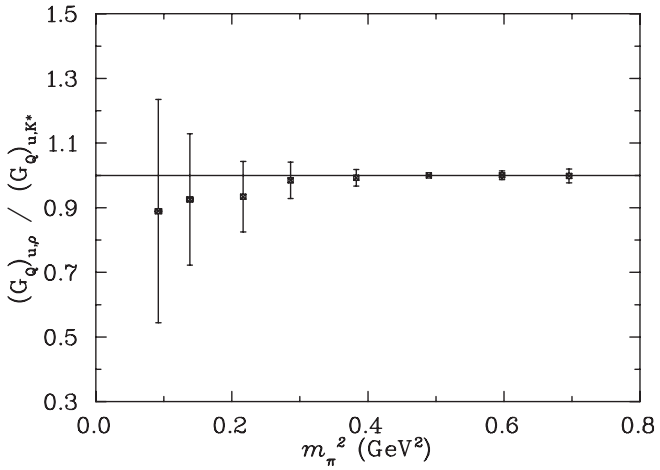

FIG. 14. Environment-dependence for light-quark contribution to vector meson quadrupole form factor.

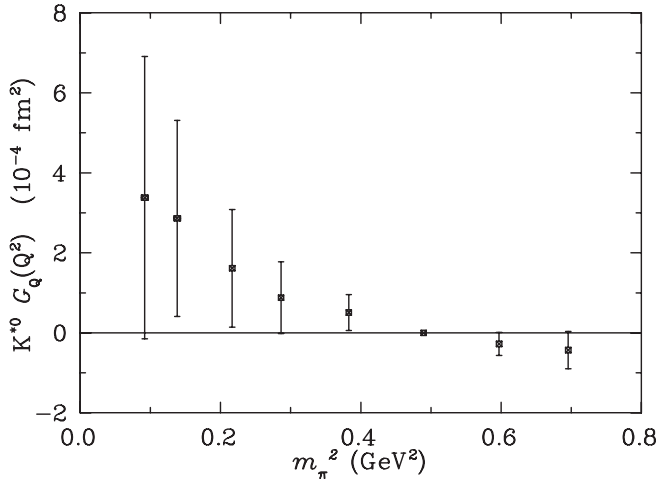

FIG. 15. Quadrupole form factor for neutral K^* meson.

TABLE VI. The quark sector contributions to the charge form factor of the pseudoscalar mesons.

m_π^2 (GeV)^2	u_π	u_K	s_K
0.6956(26)	0.833(4)	0.835(4)	0.818(4)
0.5970(26)	0.828(4)	0.830(5)	0.820(5)
0.4895(24)	0.822(5)	0.822(5)	0.822(5)
0.3828(23)	0.815(6)	0.813(6)	0.823(6)
0.2862(25)	0.810(8)	0.804(6)	0.825(6)
0.2166(27)	0.809(12)	0.798(7)	0.826(7)
0.1382(48)	0.812(22)	0.792(8)	0.826(8)
0.0920(49)	0.833(30)	0.791(8)	0.828(8)

TABLE VII. As in Fig. 6 but for the vector mesons.

m_π^2 (GeV)^2	u_ρ	u_{K^*}	s_{K^*}
0.6956(26)	0.795(5)	0.794(7)	0.771(7)
0.5970(26)	0.784(7)	0.783(8)	0.771(8)
0.4895(24)	0.769(9)	0.769(9)	0.769(9)
0.3828(23)	0.750(12)	0.754(11)	0.766(10)
0.2862(25)	0.727(18)	0.738(13)	0.760(12)
0.2166(27)	0.708(22)	0.727(15)	0.756(13)
0.1382(48)	0.683(32)	0.716(17)	0.749(15)
0.0920(49)	0.660(40)	0.707(19)	0.745(15)

TABLE VIII. The quark sector contributions to the magnetic form factor.

m_π^2 (GeV)^2	u_ρ	u_{K^*}	s_{K^*}
0.6956(26)	1.360(16)	1.373(19)	1.406(21)
0.5970(26)	1.389(19)	1.395(21)	1.413(23)
0.4895(24)	1.418(25)	1.418(25)	1.418(25)
0.3828(23)	1.455(29)	1.445(28)	1.428(27)
0.2862(25)	1.484(37)	1.469(31)	1.435(28)
0.2166(27)	1.496(47)	1.485(36)	1.438(30)
0.1382(48)	1.500(60)	1.501(41)	1.440(31)
0.0920(49)	1.483(81)	1.513(46)	1.441(33)

TABLE IX. The quark sector contributions to the quadrupole form factor.

m_π^2 (GeV)^2	u_ρ	u_{K^*}	s_{K^*}
0.6956(26)	−0.285(22)	−0.286(26)	−0.294(28)
0.5970(26)	−0.289(26)	−0.289(29)	−0.294(30)
0.4895(24)	−0.293(33)	−0.293(33)	−0.293(33)
0.3828(23)	−0.299(44)	−0.301(39)	−0.292(37)
0.2862(25)	−0.303(56)	−0.307(45)	−0.291(41)
0.2166(27)	−0.296(74)	−0.317(52)	−0.288(46)
0.1382(48)	−0.309(112)	−0.334(65)	−0.282(53)
0.0920(49)	−0.304(165)	−0.342(79)	−0.280(60)

The lattice data for the quark sector contributions to the charge form factor is contained in Tables VI and VII for the pseudoscalar and vector mesons, respectively. The magnetic and quadrupole form factors of the vector mesons is contained in Tables VIII and IX respectively.

V. CONCLUSIONS

We have established a formalism for determining the charge, magnetic and quadrupole Sachs form factors of vector mesons in lattice QCD. For the first time the electric, magnetic, and quadrupole form factors of the light vector mesons have been calculated. The electric form factor of the pseudoscalar mesons have also been calculated.

With a large lattice volume and high statistics we have resolved a clear difference between the charge radii of the pseudoscalar and vector mesons. We argue that this is consistent with quark model predictions. Furthermore, we find significant environmental sensitivity of the light-quark contributions to the charge radii of the vector mesons.

We also presented a calculation of the magnetic moments of the vector mesons. We found that the magnetic moment of the ρ^+ was consistent with the quark model predication of $1.84\mu_N$ at the $SU(3)_{\text{flavour}}$ limit. We determine that there is also an environmental sensitivity in the magnitude of the light-quark contributions to the charged vector meson magnetic moments. We argue that this is consistent with the environmental sensitivity in the light-quark contributions to the charge vector meson charge radii.

Finally, we have determined that the quadrupole form factor for a charged vector meson is negative in quenched Lattice QCD. This is consistent with previous calculations using density-density analysis. We find that the ratio of quadrupole moment to mean square charge radius is 1:30, so the deformation is small but statistically significant.

ACKNOWLEDGMENTS

We thank the Australian Partnership for Advanced Computing (APAC) and the South Australian Partnership for Advanced Computing (SAPAC) for generous grants of supercomputer time which have enabled this project. This work was supported by the Australian Research Council. J. Z. is supported by PPARC Grant No. PP/D000238/1.

[1] H.-y. Gao, Int. J. Mod. Phys. E **12**, 1 (2003).
[2] C. E. Hyde-Wright and K. de Jager, Annu. Rev. Nucl. Part. Sci. **54**, 217 (2004).
[3] J. Arrington, C. D. Roberts, and J. M. Zanotti, arXiv:nucl-th/0611050.
[4] C. F. Perdrisat, V. Punjabi, and M. Vanderhaeghen, arXiv:hep-ph/0612014.
[5] K. de Jager, arXiv:nucl-ex/0612026.
[6] R. M. Woloshyn and A. M. Kobos, Phys. Rev. D **33**, 222 (1986).
[7] W. Wilcox and R. M. Woloshyn, Phys. Rev. D **32**, 3282 (1985).
[8] R. M. Woloshyn, Phys. Rev. D **34**, 605 (1986).
[9] W. Wilcox and R. M. Woloshyn, Phys. Rev. Lett. **54**, 2653 (1985).
[10] T. Draper, R. M. Woloshyn, W. Wilcox, and K.-F. Liu, Nucl. Phys. **B318**, 319 (1989).
[11] T. Draper, R. M. Woloshyn, W. Wilcox, and K.-F. Liu, Nucl. Phys. B, Proc. Suppl. **9**, 175 (1989).
[12] Y. Nemoto (RBC), Nucl. Phys. B, Proc. Suppl. **129**, 299 (2004).
[13] J. van der Heide, J. H. Koch, and E. Laermann, Phys. Rev. D **69**, 094511 (2004).
[14] A. M. Abdel-Rehim and R. Lewis, Phys. Rev. D **71**, 014503 (2005).
[15] F. D. R. Bonnet, R. G. Edwards, G. T. Fleming, R. Lewis, and D. G. Richards (Lattice Hadron Physics), Phys. Rev. D **72**, 054506 (2005).
[16] S. Capitani, C. Gattringer, and C. B. Lang (Bern-Graz-Regensburg (BGR)), Phys. Rev. D **73**, 034505 (2006).
[17] S. Hashimoto *et al.* (JLQCD), PoS LAT2005 (2006) 336 [arXiv:hep-lat/0510085].
[18] D. Brömmel *et al.* (QCDSF/UKQCD), arXiv:hep-lat/0608021.
[19] T. Horn *et al.* (Fpi2), Phys. Rev. Lett. **97**, 192001 (2006).
[20] V. Tadevosyan *et al.* (Fpi-1), arXiv:nucl-ex/0607007.
[21] A. Samsonov, J. High Energy Phys. 12 (2003) 061.
[22] H.-M. Choi and C.-R. Ji, Phys. Rev. D **70**, 053015 (2004).
[23] V. V. Braguta and A. I. Onishchenko, Phys. Rev. D **70**, 033001 (2004).
[24] T. M. Aliev and M. Savci, Phys. Rev. D **70**, 094007 (2004).
[25] M. S. Bhagwat and P. Maris, arXiv:nucl-th/0612069.
[26] C. Alexandrou, P. de Forcrand, and A. Tsapalis, Phys. Rev. D **66**, 094503 (2002).
[27] B. G. Lasscock, J. Hedditch, D. B. Leinweber, and A. G. Williams, PoS LAT2006 (2006) 114 [arXiv:hep-lat/0611029].
[28] J. Bjorken and S. Drell, *Relativistic Quantum Fields* (McGraw-Hill, New York, 1965).
[29] S. J. Brodsky and J. R. Hiller, Phys. Rev. D **46**, 2141 (1992).
[30] R. G. Arnold, C. E. Carlson, and F. Gross, Phys. Rev. C **23**, 363 (1981).
[31] J. J. Sakurai, *Advanced Quantum Mechanics* (Addison-Wesley, Reading, MA, 1982).
[32] D. B. Leinweber, R. M. Woloshyn, and T. Draper, Phys. Rev. D **43**, 1659 (1991).
[33] S. Boinepalli, D. B. Leinweber, A. G. Williams, J. M.

Zanotti, and J. B. Zhang, Phys. Rev. D **74**, 093005 (2006).
[34] J. Litt *et al.*, Phys. Lett. **31B**, 40 (1970).
[35] D. B. Leinweber, T. Draper, and R. M. Woloshyn, Phys. Rev. D **46**, 3067 (1992).
[36] D. B. Leinweber, T. Draper, and R. M. Woloshyn, Phys. Rev. D **48**, 2230 (1993).
[37] M. Lüscher and P. Weisz, Commun. Math. Phys. **97**, 59 (1985).
[38] N. Cabibbo and E. Marinari, Phys. Lett. **119B**, 387 (1982).
[39] F. D. R. Bonnet, D. B. Leinweber, and A. G. Williams, J. Comput. Phys. **170**, 1 (2001).
[40] J. M. Zanotti *et al.* (CSSM Lattice), Phys. Rev. D **65**, 074507 (2002).
[41] J. M. Zanotti, B. Lasscock, D. B. Leinweber, and A. G. Williams, Phys. Rev. D **71**, 034510 (2005).
[42] S. Boinepalli, W. Kamleh, D. B. Leinweber, A. G. Williams, and J. M. Zanotti, Phys. Lett. B **616**, 196 (2005).
[43] W. Kamleh, D. B. Leinweber, and A. G. Williams, Phys. Rev. D **70**, 014502 (2004).
[44] T. Draper, R. M. Woloshyn, and K.-F. Liu, Phys. Lett. B **234**, 121 (1990).
[45] S. Eidelman *et al.* (Particle Data Group), Phys. Lett. B **592**, 1 (2004).
[46] W. Andersen and W. Wilcox, Ann. Phys. (N.Y.) **255**, 34 (1997).